ACS APPLIED MATERIALS & INTERFACES

Article

Ultrasensitive Enzyme-free Biosensor by Coupling Cyclodextrin Functionalized Au Nanoparticles and High Performance Au-Paper Electrode

Xiaoxiao Zheng, Li Li, Kang Cui, Yan Zhang, Lina Zhang, Shenguang Ge, and Jinghua Yu

ACS Appl. Mater. Interfaces, **Just Accepted Manuscript** • DOI: 10.1021/acsami.7b17037 • Publication Date (Web): 10 Jan 2018

Just Accepted

ACS Publications

ACS Applied Materials & Interfaces is published by the American Chemical Society.
1155 Sixteenth Street N.W., Washington, DC 20036

Ultrasensitive Enzyme-free Biosensor by Coupling Cyclodextrin Functionalized Au Nanoparticles and High Performance Au-Paper Electrode

Xiaoxiao Zheng,[†,§] Li Li,[†,§] Kang Cui,[†] Yan Zhang,[†] Lina Zhang,[‡] Shenguang Ge,*[,†] and Jinghua Yu*[,†]

[†]School of Chemistry and Chemical Engineering, University of Jinan, Jinan 250022, P. R. China

[‡]Shandong Provincial Key Laboratory of Preparation and Measurement of Building Materials, University of Jinan, Jinan 250022, P. R. China

[§]These authors contributed equally to this work.

Corresponding author:

*S. G. Ge. E-mail: chm_gesg@163.com. Phone: +86-531-82767161. Fax: +86-531-82765969.

*J. H. Yu. E-mail: ujn.yujh@gmail.com. Phone: +86-531-82767161. Fax: +86-531-82765969.

ABSTRACT: Microfluidic paper-based analytical device (μPAD), originally developed for improving healthcare in developing countries, presents a simple yet powerful platform for performing low-cost and portable diagnostic devices. Here, we reported an enzyme-free μPAD for the detection of two tumor markers. Firstly, a porous structure of gold nanoparticles (AuNPs) modified paper working electrode (Au-PWE), with a feature of all-around conductivity and plenty of active sites favoring for the biological ligands attachment, was firstly fabricated as a sensor substrate. Next cyclodextrin functionalized AuNPs (CD@AuNPs) as dual mimicking enzyme was prepared to load secondary antibodies or peptide. One the one sample zone, in the presence of carcinoembryonic antigen (CEA), CD@AuNPs could be introduced into the Au-PWE through a sandwich immunoreaction, boosting the electrochemical signal of o-phenylenediamine (o-PD) via the trigger of a cascade catalysis reaction towards glucose & o-PD, eventually resulting in a sensitive detection of CEA. On another working zone, with the introduction of another target prostate specific antigen (PSA), the peptide cleavage took place, which further led to the CD@AuNPs released from Au-PWE, and then the variation of electrochemical signals were recorded for detection of PSA. We demonstrated, using the device, the detection of CEA and PSA clinically had high sensitivity, wide linear ranges and low detection limits. We believe that our work provides a promising platform for point-of-care testing, especially in resource-limited regions.

KEYWORDS: *all-around conductivity, CD@AuNPs, cascade catalysis, point-of-care testing*

1. INTRODUCTION

Due to the ease with which they are mass-produced and functionalized, and the inherit merits of low-cost, paper-based devices have attracted considerable attentions.[1-3] In particular, microfluidic paper-based analytical devices (μPADs), proposed by Whitesides group,[4] make them more appealing to the resource-limited regions compared with traditional electrodes. To date, many of the advances in the field have arisen from studies of modifying conductive materials on the paper chips,[5-8] but it is clear that the properties of these materials are not comparable to that of the precious metal electrodes, such as gold electrodes. Therefore, in order to orient toward common applications, the conductivity of paper which greatly influences the detection sensitivity of the μPADs, has to be improved.

To tackle the issue of poor longitudinal conduction of paper chip, we employed an all-around conductive paper working electrode (PWE) based on a special and facile in-situ growth mode via gold nanoparticles (AuNPs) growing from the front to the back of the PWE. Since AuNPs, as well known by their good biocompatibility, are able to bind with many biological ligands, such as, peptide,[9] DNA[10] and proteins[11]. The successful construction of the PWE modified by AuNPs (Au-PWE) with plenty of active sites was designed to bind biological ligands, and further leading to a widened the detection linear range.

To develop and eventually achieve a new technology suitable for performance at the point of care in resource limited settings, a trend towards integrating immunosensors with different signal readout methods, such as fluorescence,[12,13]

electrochemiluminescence (ECL)[14,15] and colorimetric,[16,17] has emerged. Although great progress has been made, major technological challenges still remain, such as the requirement of sophisticated instruments in fluorescence and ECL, and semi-quantitative measurement with inaccurate results in colorimetric detection. Electrochemical biosensors, especially enzyme-based amperometric sensors, in contrast, have attracted considerable attention due to their high selectivity, sensitivity and simplicity,[18-20] aiming them to be a potential analytical method for the detection of tumor markers. However, enzyme-based electrochemical biosensors are sensitive to environmental conditions such as pH and temperature,[21] which definitely limit their applications in biomarker detections. Therefore, developing a highly efficient nonenzymic catalyst to replace enzyme is vital to promote the performance of electrochemical biosensors.

AuNPs have good catalytic activity,[22] especially when they are compounded with other materials, their catalytic properties can be greatly improved due to the synergistic effect. Recently, Zhao et al. synthesized AuNPs modified by cyclodextrin (CD@AuNPs) in a mild method by using supramolecules CD as both stabilizer and reducing agent, which exhibited mimicking properties of both glucose oxidase and horseradish peroxidase (HRP) simultaneously.[23] The novel CD@AuNPs showed a robust catalytic performance which was even better than that of enzymes, promoting it as catalyst to intensively improve the stability of the immunosensor.

In this paper, we proposed an ultrasensitive biosensor for the quantitative analysis of two tumor markers by using Au-PWE, facilitating electron transfer to improve the

sensitivity, as a sensor platform on which a large amount of biological ligands were immobilized to widen the detection range. In the presence of carcinoembryonic antigen (CEA), CD@AuNPs with double enzyme activities towards glucose and H_2O_2 was introduced into the Au-PWE through a sandwich immunoreaction, further initiating cascaded reactions between glucose and o-phenylenediamine (o-PD). Whereas the presence of prostate specific antigen (PSA) led to the breakage of the peptide and causing CD@AuNPs stripped from the PWE. Changes in the electrochemical signal produced by the redox reaction of o-PD were used to monitor this process. We demonstrate that the immunosensor has a good reproducibility, selectivity and stability, and its good performance provides a promising way for the construction of portable, facile and high-throughput μPADs.

2. EXPERIMENTAL SECTION

2.1. Materials. CD, trisodium citrate and $NaBH_4$ were purchased from Shanghai Chemical Reagent Company (Shanghai, China). CEA, primary antibodies (Ab_1), secondary antibodies (Ab_2), PSA and peptide (CEHSSKLQLAK-NH_2) were synthesized and obtained from Shanghai Linc-Bio Science Co. Ltd. 6-mercapto-1-hexanol (MCH) was received from Nanoport. Co. Ltd. (Shenzhen, China). KH_2PO_4, Na_2HPO_4, o-PD, chloroauric acid ($HAuCl_4 \cdot 4H_2O$), hydroxylammonium chloride, and glucose were acquired from Aladin Ltd. (Shanghai, China). The clinical human serum samples were ordered from Shandong Tumor Hospital. All other chemicals were of analytical grade and used without other purifications. Ultrapure water, obtained from a Lichun water purification system

(≥18.25 MΩ cm, Jinan, China), was used in this assay.

2.2. Instruments. Differential pulse voltammetric (DPV) measurements were performed on a CHI 760D electrochemical workstation (Shanghai CH Instruments Inc., China). Scanning electron microscopy (SEM) investigations were performed on a QUANTA FEG 250 thermal field emission scanning electron microscope (FEI Co., USA). Transmission electron microscopy (TEM) images were got from a JEOL 4000 EX microscope. Ultraviolet-visible (UV-vis) absorption spectra were recorded on a UV-2550 spectrophotometer (Shimadzu, Japan). X-ray photoelectron spectroscopy (XPS) measurement was performed by using a Thermofisher ESCALAB 250 X-ray photoelectron spectrometer. Fourier transform infrared (FT-IR) spectrum was obtained on a FT-IR Spectrum RX (PerkinElmer Spectoment). ^{1}H NMR spectrometry was recorded on a Bruker DPX 300 spectrometer (300 MHz).

2.3. Preparation of 3D Paper-based Electrochemical Device. In this assay, the preparation of flexible paper electrochemical device was similar to our previous work,[24] and the detail procedures were as follows. First, the shape of hydrophobic pattern on μPAD was designed using an Adobe illustrator CS4, and then the wax layer was printed on the whatman chromatography paper no. 1 with A4 size using a wax printer. Next, the wax-printed paper was hung above an electric stove for about 130 s to melt the wax, so that the wax could soakage the paper to form insulating and hydrophobic barriers. As shown in Scheme S1A, the paper device consists of a rectangle (48.0×25.0 mm) with three circles whose diameters are about 10 mm, and two rectangles (20.0×5.0 mm) containing a hydrophilic channel (5.0×2.0 mm)

respectively. The carbon counter electrode and the reference electrode are printed in the auxiliary zone and the working electrodes are printed in sample zones (Scheme S1B). After some specific modifications on the working electrode, the paper containing the hydrophilic channel was folded along the fold line to connect the two tabs. When PBS buffer solution containing glucose and o-PD was added onto the sample zone, the buffer solution would reach the paper auxiliary zone along the hydrophilic channel due to the capillary action. As a result, the three-electrode system was turned on and there would be a signal output on the electrochemical workstation.

2.4. Synthesis of CD@AuNPs and the CD@AuNPs/Ab_2 Labels. The CD@AuNPs was prepared according to the reported literature.[23] 5 mL of 0.1 M PBS (pH 7.0), 1 mL of 0.01 M $HAuCl_4$, and 10 mL of 0.01 M CD were added into 35 mL of H_2O, and then the solution was vigorously stirred. Next, the mixture was heated for 1 h under 100 °C with an oil bath. The solution would undergo a series of color changes to the final wine red, indicating the formation of CD@AuNPs (Scheme S2A). After natural cooling to room temperature, 8 mL of the above solution was collected by centrifugation for 8 min (8000 rpm) and the precipitate was re-dispersed into water (2.4 mL). Then, the CD@AuNPs/Ab_2 bioconjugates were fabricated as follows. 1.6 mL of Ab_2 (20 $\mu g \cdot mL^{-1}$) was dropped into the solution of CD@AuNPs. Under the condition of gently shaking at 4 °C for 7 h, the Ab_2 containing amino functional groups could enter into the cavity of CD to form stable host-guest inclusion complex (Scheme S2B).[25] Then the mixture was centrifuged at 10000 rpm for 5 min and further washed with PBS buffer solution (pH 7.4) for three times. Finally, the signal

labels were re-dispersed in 4 mL of PBS buffer solution and stored at a refrigerator when not in use.

2.5. Fabrication of Au-PWE. The Au-PWE with the feature of all-around conductivity was fabricated according to the literature with appropriate modifications.[26] First, the gold seeds were prepared by using $NaBH_4$ and sodium citrate as reductant and stabilizer, respectively. Next, about 60.0 μL of gold seeds was dropped into the bare sample zone and equilibrated at ambient temperature until the paper chip was dry. The steps were repeated three times. After rinsing with water thoroughly, 60.0 μL of freshly prepared gold-growth aqueous solution (the mixture of 200 mM hydroxylammonium chloride and 1% $HAuCl_4$) was applied for AuNPs growth. 30 min later, the PWE was washed with water again. Then, the above mentioned steps were repeated for one time. In the second iteration, the gold seeds and the gold-growth aqueous solution would pass through the paper chip to reach the other side due to the capillary action and gravity to complete the double-faced growth. Thus porous Au-PWE with all-around conductivity was obtained.

2.6. Fabrication of the immunosensor. Briefly, on the one sample zone, Ab_1 (60 μL, 20 $\mu g \cdot mL^{-1}$) was modified on the Au-PWE through chemical absorption between AuNPs and the amino of Ab_1, and incubated for about 40 min. Then, 1% bovine serum albumin (BSA) solution was dropped on the paper sample zone for 1 h to block the possible remaining active sites against nonspecific adsorption. On another sample zone, 60 μL of peptide (10 μM) was added to the Au-PWE and incubated at room temperature for about 1 h to conjugate with porous AuNPs through Au-S bond. 1 mM

MCH was used to block the possible nonspecific sites on the peptide/Au-PWE. After incubated for 30 min, the CD@AuNPs was immobilized on the peptide. After every step, the modified Au-PWE should be washed with washing buffer solution entirely. Finally, the obtained immunosensor towards the detection of CEA and PSA was stored in a refrigerator at 4 °C prior to electrochemical detection.

2.7. Immunoassay Procedure of the μPAD. The immunoassay procedures were shown in Scheme 1. As shown in Scheme 1B, at room temperature, 40 μL of standard solution of CEA with various concentrations was dipped on the paper sample zone and incubated for about 1 h, followed by washing with buffer solution. Next, 60 μL of CD@AuNPs/Ab_2 bioconjugates solution was added into the CEA/Ab_1/Au-PWE to incubate for another 1 h. After washing with buffer solution, the paper chip containing hydrophilic channel was folded along the fold line. Then, the μPAD was connected to electrochemical workstation and the measurements were carried out in 50 μL of PBS solution (0.01 M, pH 7.4), which containing 0.28 μmol glucose and 0.25 μmol o-PD. A DPV measurement from -0.45 to -0.68 V with width of 0.05 s and pulse amplitude of 0.05 V was performed to record the amperometric responses (Scheme 1C).

As shown in Scheme 1D, the above μPAD was further used to detect PSA through another detection zone. First, 40 μL of PSA standard solution with various concentrations was dropped into the paper sample zone to incubate 40 min. After washing with PBS solution thoroughly to rush the cleaved CD@AuNPs from peptides, electrochemical measurements were carried out on a workstation. According to the decreasing of the signal, the content of PSA could be obtained (Scheme 1E).

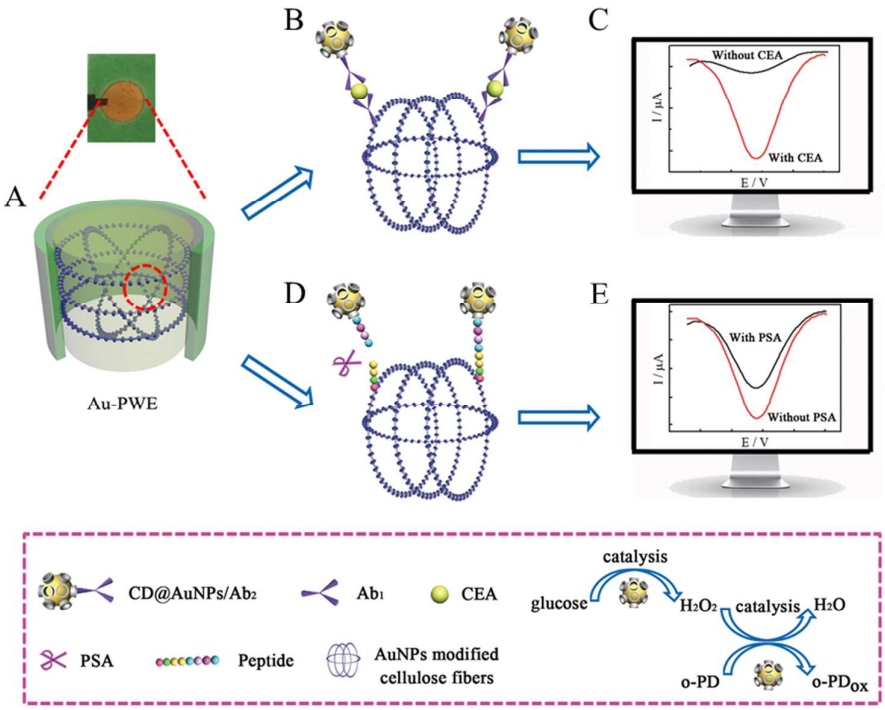

Scheme 1. Schematic of the Immunosensor for the Detection of CEA and PSA. (A) Au-PWE; detection mechanism of the CEA (B) and PSA (D); signal responses toward CEA (C) and PSA (E).

3. RESULTS AND DISCUSSION

3.1. Characterization of Au-PWE. As we all know, paper is porous with much rough cellulose fibers (Figure 1A), which can offer an excellent adsorption microenvironment for gold seeds.[27] After incubated in gold-growth solution, the dense and continuous AuNPs on the surfaces of cellulose fibers are observed in Figure 1B&D compared with bare PWE (Figure 1A and 1C). Plenty of holes were found at the morphology of AuNPs (Figure 1E), indicating a kiwi-fruit likely porous structure of the AuNPs. And the diameters of AuNPs are mainly distributed in the range of 100-150 nm. The cross-section of Au-PWE (Figure 1F) shows AuNPs also filling inside of the porous structure. The unique all-around conductive Au-PWE obtained

through an in-situ growth process could greatly improve the sensitivity of the paper chip.

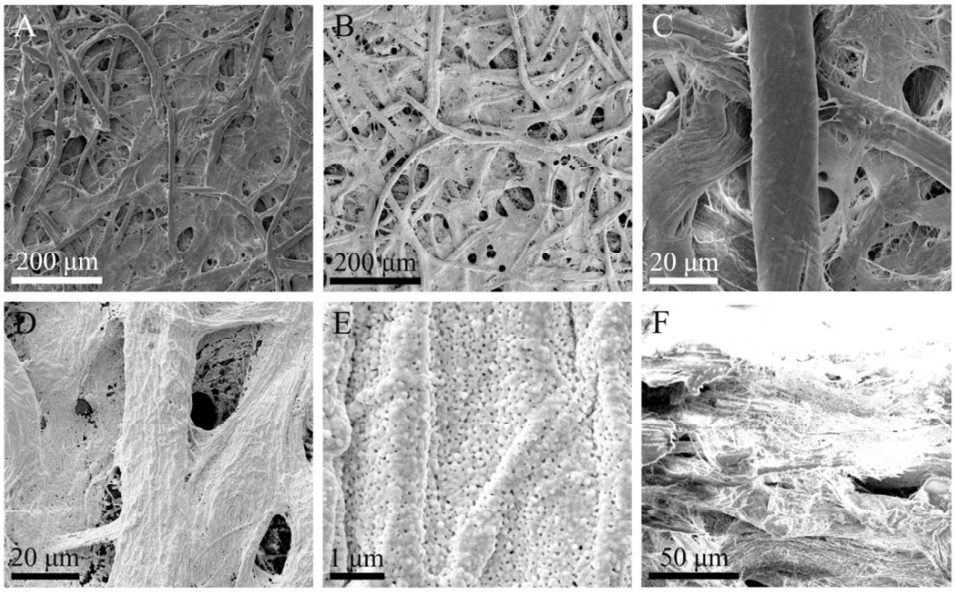

Figure 1. SEM images of (A) bare PWE; (B) Au-PWE; (C) enlarged cellulose fibers in the bare PWE; (D and E) enlarged Au-PWE with different magnifications; (F) the cross-section of Au-PWE.

In order to verify properties of the designed paper chip, its conductivity, a bottleneck problem for hindering paper chip sensitivity, was firstly measured by an Agilent U1251B multi-meter (Figure S1A). Owing to the successful growth of porous AuNPs on the front and back surfaces of paper chip, the longitudinal resistance of Au-PWE is as low as 0.66 Ω (Figure S1B). Further, a four-probe tester is employed here to measure the resistance of Au-PWE and a new clean ITO, respectively (Figure 2A and 2C). As can be seen from Figure 2B, the resistance of a bare ITO is 1.253 Ω, while the Au-PWE is only 0.1878 Ω (Figure 2D). Therefore, according to the

resistivity formula, resistivity of this ITO could be easily calculated as 6.15×10^{-5} Ω cm, and that of Au-PWE was 9.17×10^{-6} Ω cm, indicating that the conductivity of Au-PWE we fabricated was significantly better than that of ITO. In addition, the conductivity of the obtained Au-PWE was close to the pure Au (2.4×10^{-6} Ω cm), which could be attributed to the large surface area and porous structure of the paper providing good environment for the growth of AuNPs. All the results revealed that the paper chip we designed had a much better conductivity than that of previous prepared functionalized paper chips.[26]

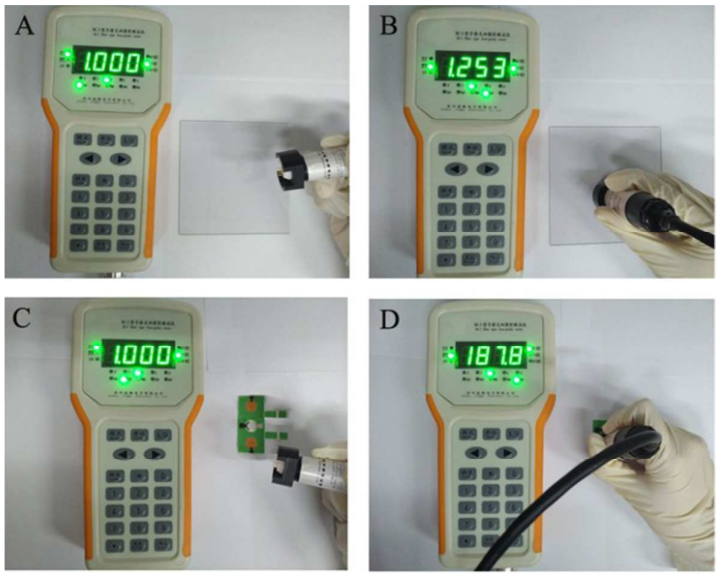

Figure 2. Four-probe tester is used to detect the resistance of ITO (A and B), and the Au-PWE (C and D), respectively.

3.2. Characterization of CD@AuNPs. To verify the successful synthesis of CD@AuNPs, different technologies were used to characterize the material.[23] The Figure 3A and 3B are TEM images of CD@AuNPs, showing that the size of the

material is about 24 nm in diameter. The wine red CD@AuNPs solution is characterized with UV-vis absorbing spectra (Figure 3C), showing a strong absorbing peak at 520 nm which is the typical feature of gold nanospheres. The structure of CD and CD@AuNPs were characterized with FT-IR spectrum (Figure 4A). By comparing the two curves in Figure 4A, typical functional groups of CD are retained in the obtained CD@AuNPs. The difference is that the hydroxyl band (3354.7 cm^{-1}) of CD@AuNPs is much narrower than that of CD, indicating that the hydroxyl groups are decreased after the reaction. XPS was further used to characterize the structure of the product. Three peaks, 530.1, 532.8 and 531.9 eV, are observed in O 1s XPS spectra (Figure 4B) and they are resulted from C=O, O-C=O/C-O-C, and C-O respectively. However, four peaks are exhibited in C 1s spectra (Figure 4C) and they are attributed to O-C-O/C=O (287.6 eV), C-C (284.7 eV), O-C=O (288.5 eV) and C-OH (286.5 eV). The XPS data in Figure 4C and Figure 4D shows that carboxyl groups are produced in the reaction of CD and $HAuCl_4$. What's more, the formed carboxyl groups could interact with AuNPs surface by forming O-Au conjunction, so that CD was connected to the surface of AuNPs. As shown in Figure 4E, there are six different chemical shifts in ^1H NMR spectra, corresponded well with CD molecules themselves (Figure 4F). This result indicated that the macrocycle structure of CD remained well after the reaction. All of the characterization data demonstrated that CD@AuNPs was successfully synthesized through a mild method.

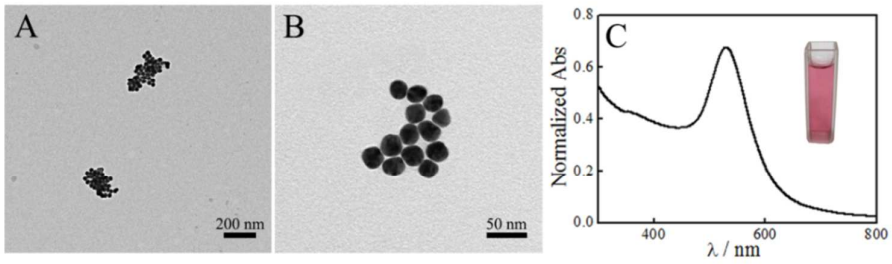

Figure 3. (A and B) TEM images of CD@AuNPs under different magnifications. (C) The UV-vis spectrum of the CD@AuNPs. Inset photo: CD@AuNPs solution.

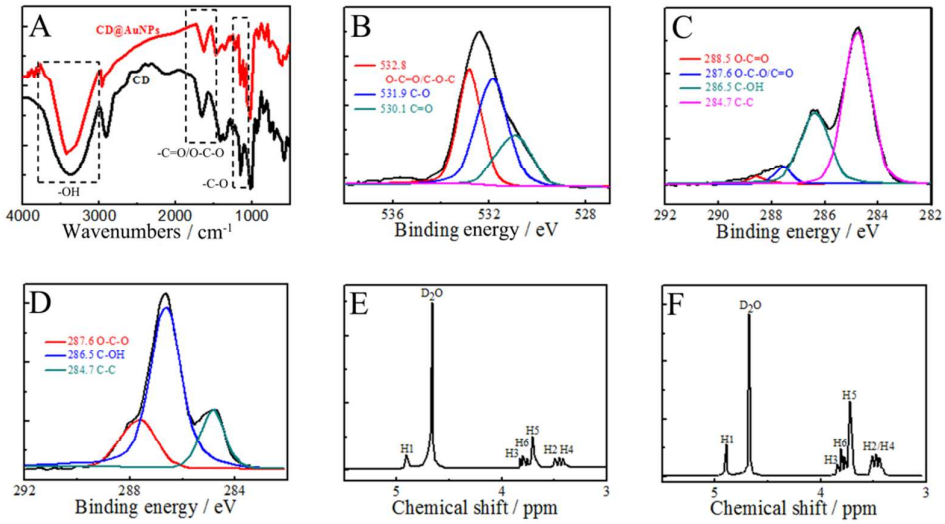

Figure 4. (A) FT-IR spectra of CD@AuNPs (red curve) and CD (black curve). (B) High-resolution XPS survey scan of O 1s of the CD@AuNPs. (C and D) High-resolution XPS survey scan of C 1s of CD@AuNPs and CD, respectively. (E and F) ^{1}H NMR spectrum (in D_2O) of CD@AuNPs and CD, respectively.

3.3. Optimization of the Detection Conditions. The DPV peak current was significantly influenced by the pH value. Figure 5A shows the effect of pH on the current response towards 1.0 ng·mL^{-1} CEA. The peak current increases continuously from 5.9 to 7.4 until 7.4 to reach the maximum, and then begins to decline. As a result, pH 7.4 PBS buffer solution was selected as the optimal electrolyte solution to detect

the content of CEA. As shown in Figure 5B, the PBS buffer solution of pH 7.4 was also used for the detection of PSA.

The incubation time of the peptide and PSA was very important in this assay, which directly determined whether the experiment towards PSA was successful or not. Therefore, it was necessary to investigate the optimal reaction time of the peptide modified Au-PWE in PSA solution. At room temperature, the peak current for PSA (1.0 ng·mL^{-1}) increases before the reaction time up to 40 min and then reaches a plateau after 40 min (Figure 5C), indicating that the binding between peptide and PSA is saturated. Consequently, 40 min of reaction time was used for the optimal time.

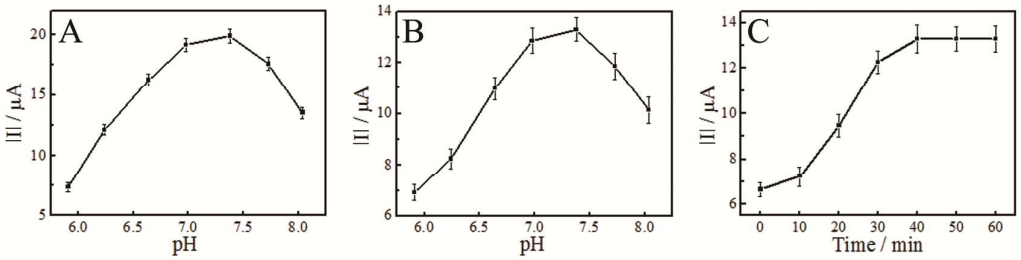

Figure 5. (A and B) Effects of pH on the current responses for 1.0 ng·mL^{-1} CEA and 1.0 ng·mL^{-1} PSA, respectively. (C) Optimization of the incubation time of PSA.

3.4. Performance of the μPAD. After introduction of CD@AuNPs/Ab_2 bioconjugates into the CEA/Ab_1/Au-PWE, there would be a sandwich immunoreaction occurs (Scheme 1B). The electrochemical impedance spectroscopy (EIS) (Figure S2A) and cyclic voltammetry (CV) measurements (Figure S2B) were used to demonstrate the successful construction of the μPAD. Under optimal experimental conditions, a DPV peak, generated by the electroactive species

2,2'-diaminoazobenzene, is appeared, which is much higher than nonspecific absorption of CD@AuNPs/Ab_2 in Ab_1/Au-PWE (Scheme 1C), suggesting that the nonspecific sites are very little in the absence of CEA. The detection mechanism of this assay was that glucose could be catalytically oxidized in the presence of CD@AuNPs to generate H_2O_2 and gluconic acid. Then the former reacted with o-PD to generate 2,2'-diaminoazobenzene. The equation of the reaction was shown below:

$$\text{glucose}+O_2 \xrightarrow{\text{CD@AuNPs}} \text{gluconic acid}+H_2O_2$$

$$\text{o-PD}+H_2O_2 \xrightarrow{\text{CD@AuNPs}} \text{2,2'-diaminoazobenzene}+H_2O$$

The reason for the cascade reaction was that CD@AuNPs possessed unpredictable catalytic activity and exhibited mimicking properties of both glucose oxidase and HRP simultaneously.[23] To prove the CD@AuNPs have double enzyme activities, the kinetic data were obtained by varying one substrate concentration while keeping the other substrate concentration constant (more detailed procedures are shown in Supporting Information). The catalytic process can be well-described by the Michaelis-Menten curve (Figure S3), and the kinetic parameters are shown in Table S1 and S2. Furthermore, the response to 2,2'-diaminoazobenzene was related to the quantity of the CD@AuNPs/Ab_2, which depended on the amount of CEA. With increasing of CEA concentration, the DPV signal increases significantly (Figure 6A). As shown in Figure 6B, a good linear correlation is achieved between the current difference and the concentration of CEA within the detection range of 0.005 to 100 $ng \cdot mL^{-1}$. The equation is $\Delta I = 12.81 + 4.04 \lg[C_{CEA}\,(ng \cdot mL^{-1})]$ with a correlation

coefficient of 0.997 (n=10). What's more, the detection limit was about 0.002 ng·mL^{-1} at a signal-to-noise ratio of 3. Particularly, this assay has a larger linear range and a much lower detection limit when compared with other proposed assays for the detection of CEA (Table 1).

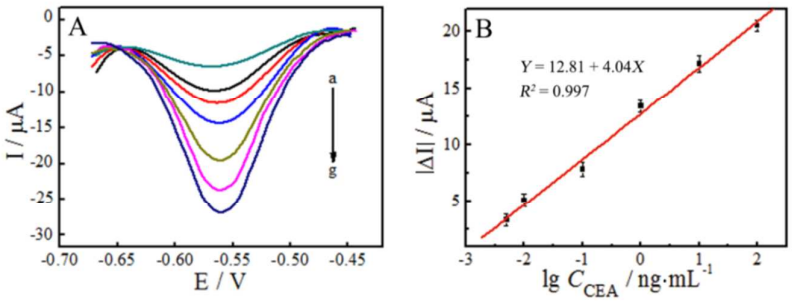

Figure 6. (A) Different DPV responses of the proposed μPAD in 50 μL of PBS buffer solution (pH 7.4) containing 0.25 μmol o-PD and 0.28 μmol glucose with CEA concentration increasing from (a) to (g) (0.00, 0.005, 0.01, 0.10, 1.00, 10.0, 100 ng·mL^{-1}). (B) Linear relationship between the logarithm of CEA concentration and the peak current difference of DPV.

Table 1. Comparison of the Proposed μPAD with Other Methods for the Detection of CEA

Detection methods	Linear range (ng·mL^{-1})	Detection limit (ng·mL^{-1})	References
CV	1.5-200	0.05	28
Fluorescence	0.05-20	0.0067	12
ECL	0.01-50	0.006	29
Photoelectrochemical	0.05-20	0.01	30
DPV	0.005-100	0.002	This work

In the detection of PSA (Scheme 1D and E), the DPV peak decreases with the increasing concentration of PSA (Figure 7A). The calibration plot in Figure 7B shows a good linear relationship between the current difference and the logarithm of PSA

concentration in the range from 0.002 to 40.00 ng·mL^{-1} with a correlation coefficient of 0.993 (n=10). And the equation is $\Delta I = 17.49 + 4.38 \lg[C_{PSA}(\text{ng·mL}^{-1})]$. In addition, the performance of the proposed μPAD in this article for PSA detection has also been compared with other reported assays and the results are summarized in Table 2. From Table 2, the μPAD shows a wider detection linear range and a lower detection limit (0.001 ng·mL^{-1}) at a signal-to-noise ratio of 3. All the results provided powerful evidence that our strategy had highly sensitivity for detection of PSA.

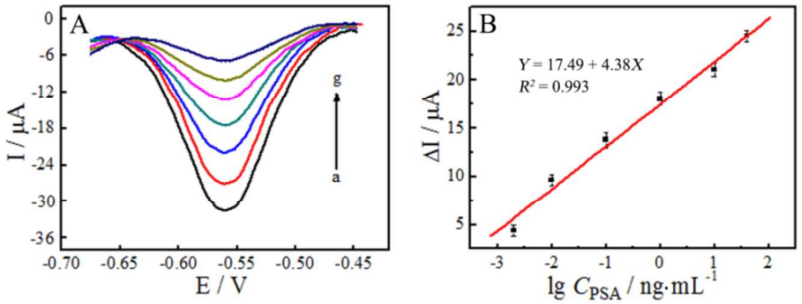

Figure 7. (A) Typical DPV curves of μPAD for the different concentrations of PSA (ng·mL^{-1}) from a to g: (a) 0.00, (b) 0.002, (c) 0.010, (d) 0.100, (e) 1.00, (f) 10.0, (g) 40.0. (B) Calibration curve of the current difference vs the logarithmic value of PSA concentration.

Table 2. Comparison of Different Immunodevices for the Detection of PSA

Detection method	Linear range (ng·mL^{-1})	Detection limit (ng·mL^{-1})	References
ECL	0.01-50	0.003	29
Photoelectrochemical	0.01-80	0.003	31
Linear sweep voltammetry	0.001-30	0.0007	32
Colorimetric Immunoassay	0.05-20	0.03	33
DPV	0.002-40	0.001	This work

3.5. Reproducibility, Selectivity and Stability of this μPAD. Intra- and inter-assay relative standard deviations (RSD) were used to evaluate the reproducibility of this

μPAD. The RSD, firstly using CEA as a model, for six times parallel tests in the same one paper sample zone (intra-assay) incubated in the incubating solution containing 1.0 ng·mL^{-1} CEA, was 5.1%. The detection of 1.0 ng·mL^{-1} CEA on six different paper sample zones at the same conditions showed the RSD of 5.9%. Secondly, using PSA as a model, the RSD of the intra-assay and inter-assay were 6.5% and 5.5%, respectively. All the RSD results indicated that the reproducibility of the μPAD was acceptable.

Human alphafetoprotein (AFP), casein and BSA, as possible interferences, were used to evaluate the specificity of the proposed μPAD. As shown in Figure S4A, when Ab_1/Au-PWE is incubated with 100 ng·mL^{-1} AFP, casein and BSA solution, respectively, a similar current intensity with that of the background is exhibited, while only the current of CEA shows an obvious increase. Importantly, the response of μPAD to the mixture including the interfering components and CEA is almost the same as that with only CEA. The same method was applied to detect the specificity of μPAD towards the detection of PSA (Figure S4B). All the results showed that the proposed μPAD had an excellent specificity for CEA and PSA. After the μPAD was stored at 4 °C in a dry environment for 3 days, no detectable loss of the initial responses was observed. And after 15 days, it still could retain 91.2% and 90.3% of the initial responses for a same concentration of CEA and PSA, respectively, suggesting that the stability of this μPAD was acceptable.

3.6. Analysis of Clinical Serum Specimens. We diluted different concentrations of CEA and PSA solution in human serum samples and then measured their recoveries.

The obtained results about CEA are showed in Table S3. It can be seen that the recoveries about CEA is in the range of 100.4% to 109.2% and that of PSA is 100.9% to 114.0% (Table S4). The RSD values of CEA and PSA are from 3.51% to 5.43% and 2.96% to 4.85%, respectively. All the results indicated that the proposed μPAD had a great potential application towards the detection of CEA and PSA clinically.

4. CONCLUSION

In conclusion, with the CEA-induced sandwich immunoreaction and the PSA-induced cleave of the special peptide, a novel and ultrasensitive μPAD had been constructed successfully for high-throughput detection of CEA and PSA. We demonstrated the Au-PWE with all-around conductivity not only accelerated the electron transfer but also provided more active sites for biological ligands attachment, and CD@AuNPs with dual enzyme activities as catalyst could reduce the amount of enzymes, greatly improving the stability of the immunosensor. Also, as our device with good reproducibility and selectivity provides analytical performance sufficient for clinical assays of the two tumor markers, we believe that this facile μPAD with high sensitivity and widened the detection linear range will lay a good foundation for the development of portable devices in diagnosis of diseases.

ASSOCIATED CONTENT

Supporting Information

Kinetic analysis of the CD@AuNPs catalysis, characterization of the modified PWE, scheme of the designed 3D paper electrochemical device, schematic of the detailed

process of the formation of CD@AuNPs and CD@AuNPs/Ab_2, investigations of the longitudinal resistance of the Au-PWE, EIS and CVs of the different modification process of the PWE, the selectivity of the proposed μPAD towards CEA and PSA, respectively, experimental data of the determination of CEA (and PSA) added in serum.

AUTHOR INFORMATION

Corresponding Authors

*S. G. Ge. E-mail: chm_gesg@163.com. Phone: +86-531-82767161. Fax: +86-531-82765969.

*J. H. Yu. E-mail: ujn.yujh@gmail.com. Phone: +86-531-82767161. Fax: +86-531-82765969.

Author Contributions

[§]X. X. Z. and L. L. contributed eaually to this work.

Notes

The authors declare no competing financial interest.

ACKNOWLEDGMENTS

This work was financially supported by the program of Taishan Scholars, and the National Natural Science Foundation of China (21775055, 21475052).

REFERENCES

(1) Bruzewicz, D. A.; Reches, M.; Whitesides, G. M. Low-Cost Printing of Poly (dimethylsiloxane) Barriers to Define Microchannels in Paper. *Anal. Chem.* **2008**, *80*, 3387-3392.

(2) Yang, Y. Y.; Noviana, E.; Nguyen, M. P.; Geiss, B. J.; Dandy, D. S.; Henry, C. S. Paper-Based Microfluidic Devices: Emerging Themes and Applications. *Anal. Chem.* **2017**, *89*, 71-91.

(3) Tian, T.; An, Y.; Wu, Y. P.; Song, Y. L.; Zhu, Z.; Yang, C. Y. Integrated Distance-Based Origami Paper Analytical Device for One-Step Visualized Analysis. *ACS Appl. Mater. Interfaces* **2017**, *9*, 30480-30487.

(4) Martinez, A. W.; Phillips, S. T.; Butte, M. J.; Whitesides, G. M. Patterned Paper as a Platform for Inexpensive, Low-Volume, Portable Bioassays. *Angew. Chem. Int. Ed.* **2007**, *46*, 1318-1320.

(5) Wu, Y. F.; Xue, P.; Kang, Y. J.; Hui, K. M. Paper-Based Microfluidic Electrochemical Immunodevice Integrated with Nanobioprobes onto Graphene Film for Ultrasensitive Multiplexed Detection of Cancer Biomarkers. *Anal. Chem.* **2013**, *85*, 8661-8668.

(6) Li, L.; Zhang, L. N.; Yu, J. H.; Ge, S. G.; Song, X. R. All-graphene composite materials for signal amplification toward ultrasensitive electrochemical immunosensing of tumor marker. *Biosens. Bioelectron.* **2015**, *71*, 108-114.

(7) Li, L.; Zhang, Y.; Zhang, L. N.; Ge, S. G.; Liu, H. Y.; Ren, N.; Yan, M.; Yu, J. H. Paper-Based Device for Colorimetric and Photoelectrochemical Quantification of the Flux of H_2O_2 Releasing from MCF-7 Cancer Cells. *Anal. Chem.* **2016**, *88*, 5369-5377.

(8) Ge, S. G.; Wu, K. Q.; Zhang, Y.; Yan, M.; Yu, J. H. Paper-based biosensor relying on flower-like reduced graphene guided enzymatically deposition of polyaniline for Pb^{2+} detection. *Biosens. Bioelectron.* **2016**, *80*, 215-221.

(9) Koleva, B. B.; Zareva, S.; Kolev, T.; Spiteller, M. New Au (Ⅲ), Pt (Ⅱ) and Pd (Ⅱ) complexes with glycyl-containing homopeptides. *J. Coord. Chem.* **2008**, *61*, 3534-3548.

(10) Marcon, G.; Carotti, S.; Coronnello, M.; Messori, L.; Mini, E.; Orioli, P.; Mazzei, T.; Cinellu, M. A.; Minghetti, G. Gold (Ⅲ) Complexes with Bipyridyl Ligands: Solution Chemistry, Cytotoxicity, and DNA Binding Properties. *J. Med. Chem.* **2002**, *45*, 1672-1677.

(11) Casini, A.; Hartinger, C.; Gabbiani, C.; Mini, E.; Dyson, P. J.; Keppler, B. K.; Messori, L. Gold (Ⅲ) compounds as anticancer agents: Relevance of gold-protein interactions for their mechanism of action. *J. Inorg. Biochem.* **2008**, *102*, 564-575.

(12) Qiu, Z. L.; Shu, J.; Tang, D. P. Bioresponsive Release System for Visual Fluorescence Detection of Carcinoembryonic Antigen from Mesoporous Silica Nanocontainers Mediated Optical Color on Quantum Dot-Enzyme-Impregnated Paper. *Anal. Chem.* **2017**, *89*, 5152-5160.

(13) Liu, D. B.; Huang, X. L.; Wang, Z. T.; Jin, A.; Sun, X. L.; Zhu, L.; Wang, F.; Ma, Y.; Niu, G.; Walker, A. R. H.; Chen, X. Y. Gold Nanoparticle-Based Activatable Probe for Sensing Ultralow Levels of Prostate-Specific Antigen. *ACS Nano* **2013**, *7*, 5568-5576.

(14) Chen, L. C.; Zeng, X. T.; Si, P.; Chen, Y. M.; Chi, Y. W.; Kim, D. H.; Chen, G. N. Gold Nanoparticle-Graphite-Like C_3N_4 Nanosheet Nanohybrids Used for Electrochemiluminescent Immunosensor. *Anal. Chem.* **2014**, *86*, 4188-4195.

(15) Sardesai, N. P.; Barron, J. C.; Rusling, J. F. Carbon Nanotube Microwell Array for Sensitive Electrochemiluminescent Detection of Cancer Biomarker Proteins. *Anal. Chem.* **2011**, *83*, 6698-6703.

(16) Liu, W.; Guo, Y. M.; Zhao, M.; Li, H. F.; Zhang, Z. J. Ring-Oven Washing Technique Integrated Paper-based Immunodevice for Sensitive Detection of Cancer Biomarker. *Anal. Chem.* **2015**, *87*, 7951-7957.

(17) Qu, F. l.; Li, T.; Yang, M. H. Colorimetric platform for visual detection of cancer biomarker based on intrinsic peroxidase activity of graphene oxide. *Biosens. Bioelectron.* **2011**, *26*, 3927−3931.

(18) Wu, H.; Fan, S. H.; Jin, X. Y.; Zhang, H.; Chen, H.; Dai, Z.; Zou, X. Y. Construction of a Zinc Porphyrin-Fullerene-Derivative Based Nonenzymatic Electrochemical Sensor for Sensitive Sensing of Hydrogen Peroxide and Nitrite. *Anal. Chem.* **2014**, *86*, 6285-6290.

(19) Su, B. L.; Tang, D. P.; Li, Q. F.; Tang, J.; Chen, G. N. Gold-silver-graphene hybrid nanosheets-based sensors for sensitive amperometric immunoassay of alpha-fetoprotein using nanogold-enclosed titania nanoparticles as labels. *Ana. Chim. Acta* **2011**, *692*, 116-124.

(20) Ronkainen, N. J.; Okon, S. L. Nanomaterial-Based Electrochemical Immunosensors for Clinically Significant Biomarkers. *Materials* **2014**, *7*, 4669-4709.

(21) Mu, Y.; Jia, D. L.; He, Y. Y.; Miao, Y. Q.; Wu, H. L. Nano nickel oxide modified non-enzymatic glucose sensor with enhanced sensitivity through an electrochemical process strategy at high potential. *Biosens. Bioelectron.* **2011**, *26*, 2948-2952.

(22) Daniel, M. C.; Astruc, D. Gold Nanoparticles: Assembly, Supramolecular Chemistry, Quantum-Size-Related Properties, and Applications toward Biology, Catalysis, and Nanotechnology. *Chem. Rev.* **2004**, *104*, 293-346.

(23) Zhao, Y.; Huang, Y. C.; Zhu, H.; Zhu, Q. Q.; Xia, Y. S. Three-in-One, Sensing, Self-Assembly, and Cascade Catalysis of Cyclodextrin Modified Gold Nanoparticles. *J. Am. Chem. Soc.* **2016**, *138*, 16645-16654.

(24) Ge, L.; Wang, S. M.; Song, X. R.; Ge, S. G.; Yu, J. H. 3D Origami-based multifunction-integrated immunodevice: low-cost and multiplexed sandwich

chemiluminescence immunoassay on microfluidic paper-based analytical device. *Lab. Chip* **2012**, *12*, 3150-3158.

(25) Jiang, L. P.; Han, J.; Li, F. Y.; Gao, J.; Li, Y. Y.; Dong, Y. H.; W, Q. A sandwich-type electrochemical immunosensor based on multiple signal amplification for α-fetoprotein labeled by platinum hybrid multiwalled carbon nanotubes adhered copper oxide. *Elec. Acta* **2015**, *160*, 7-14.

(26) Yan, J. X.; Yan, M.; Ge, L.; Yu, J. H.; Ge, S. G.; Huang, J. D. A microfluidic origami electrochemiluminescence aptamer-device based on a porous Au-paper electrode and a phenyleneethynylene derivative. *Chem. Comm.* **2013**, *49*, 1383-1385.

(27) Li, L.; Xu, J. M.; Zheng, X. X.; Ma, C.; Song, X. R.; Ge, S. G.; Yu, J. H.; Yan, M. Growth of gold-manganese oxide nanostructures on a 3D origami device for glucose-oxidase label based electrochemical immunosensor. *Biosens. Bioelectron.* **2014**, *61*, 76-82.

(28) Tang, D. P.; Yuan, R.; Chai, Y. Q. Magnetic Core-Shell Fe_3O_4@Ag Nanoparticles Coated Carbon Paste Interface for Studies of Carcinoembryonic Antigen in Clinical Immunoassay. *J. Phys. Chem. B.* **2006**, *110*, 11640-11646.

(29) Zhang, Y.; Liu, W. Y.; Ge, S. G.; Yan, M.; Wang, S. W.; Yu, J. H.; Li, N. Q.; Song, X. R. Multiplexed sandwich immunoassays using flow-injection electrochemiluminescence with designed substrate spatial-resolved technique for detection of tumor markers. *Biosens. Bioelectron.* **2013**. *41*, 684-690.

(30) Tu, W. W.; Wang, W. J.; Lei, J. P.; Deng, S. Y.; Ju, H. X. Chemiluminescence excited photoelectrochemistry using graphene-quantum dots nanocomposite for biosensing. *Chem. Commun.* **2012**, *48*, 6535-6537.

(31) Shu, J.; Qiu, Z. L.; Zhou, Q.; Lin, Y. X.; Lu, M. H.; Tang, D. P. Enzymatic Oxydate-Triggered Self-llluminated Photoelectrochemical Sensing Platform for Portable Immunoassay Using Digital Multimeter. *Anal. Chem.* **2016**, *88*, 2958-2966.

(32) He, Y.; Xie, S. B.; Yang, X.; Yuan, R.; Chai, Y. Q. Electrochemical Peptide Biosensor Based on in Situ Silver Deposition for Detection of Prostate Specific Antigen. *ACS Appl. Mater. Interfaces* **2015**, *7*, 13360-13366.

(33) Gao, Z. Q.; Xu, M. D.; Hou, L.; Chen, G. N.; Tang, D. P. Magnetic Bead-Based Reverse Colorimetric Immunoassay Strategy for Sensing Biomolecules. *Anal. Chem.* **2013**, *85*, 6945-6952.

Graphic for manuscript

Ultrasensitive Enzyme-free Biosensor by Coupling Cyclodextrin Functionalized Au Nanoparticles and High Performance Au-Paper Electrode

Xiaoxiao Zheng,[†,§] Li Li,[†,§] Kang Cui,[†] Yan Zhang,[†] Lina Zhang,[‡] Shenguang Ge,*[,†] and Jinghua Yu*[,†]

[†]School of Chemistry and Chemical Engineering, University of Jinan, Jinan 250022, P. R. China

[‡]Shandong Provincial Key Laboratory of Preparation and Measurement of Building Materials, University of Jinan, Jinan 250022, P. R. China